Zhao *et al. Journal of Nanobiotechnology* (2025) 23:366
https://doi.org/10.1186/s12951-025-03460-5

Journal of Nanobiotechnology

RESEARCH Open Access

A self-assembled multicomponent RNA nano-biopesticide for increasing the susceptibility of destructive bean flower thrips to insecticides via ds*Nrf2*

Jiajia Zhao[1,2], Zeng Wang[2], Jiaming Yin[1,2], Ying Wei[2], Mingshan Li[2], Zhongzheng Ma[3], Meizhen Yin[4], Min Dong[1,2], Jie Shen[1,2] and Shuo Yan[1,2*]

Abstract

High resistance of bean flower thrips (BFT, *Megalurothrips usitatus*) has led to the unscientific application of insecticides to cause famous "toxic cowpea" incidents in China. Nuclear factor erythroid 2-related factor 2 (Nrf2) plays an important role in inducing antioxidant responses and drug detoxification. Therefore, the detoxification genes may be suppressed to control insecticide resistance via Nrf2. Herein, we demonstrated that the expression of most detoxification genes and enzyme activity were remarkably suppressed via *nrf2* RNAi. Subsequently, a novel hydrophilic-lipophilic diblock polymer (HLDP) was developed to co-assemble with ds*Nrf2* and sulfoxaflor (SUL) into nanoscale SUL/HLDP/ds*Nrf2* complex (221.52 nm). Excitingly, the SUL/HLDP/ds*Nrf2* complex exhibited excellent leaf adhesion performance, with the smaller contact angle, reduced surface tension, amplified contact area, improved retention, and enhanced plant uptake. Meanwhile, theSUL/HLDP/ds*Nrf2* displayed high delivery efficiency in vitro and in vivo, and its insecticidal activity against BFTs was significantly higher than SUL. Furthermore, the required doses of SUL/HLDP/ds*Nrf2* to achieve similar insecticidal activity were 50.14% and 58.42% of SUL via immersion and oral feeding, respectively. Overall, this study elucidated the regulatory role of *nrf2* in the detoxification and metabolism of BFTs and developed a self-assembled multicomponent RNA nano-biopesticide to increase the susceptibility of BFTs to insecticides.

Keywords Co-delivery system, Drug adjuvant, Gene nanocarrier, Multicomponent RNA nano-biopesticide, Increased insecticide susceptibility

*Correspondence:
Shuo Yan
yanshuo2011@foxmail.com
[1]Sanya Institute of China Agricultural University, Sanya 572025, PR China
[2]State Key Laboratory of Agricultural and Forestry Biosecurity, Department of Plant Biosecurity, College of Plant Protection, China Agricultural University, Beijing 100193, China
[3]Institute of Plant Protection, Beijing Academy of Agriculture and Forestry Sciences, Beijing 100097, PR China
[4]State Key Laboratory of Chemical Resource Engineering, Beijing Lab of Biomedical Materials, Beijing University of Chemical Technology, Beijing 100029, PR China

Introduction

Cowpeas produced in the Hainan province of China have been repeatedly found to contain residues of highly toxic banned pesticides since 2010, leading to a series of "toxic cowpea" incidents [1]. This not only poses a threat to human health but also has a continuous negative impact on vegetable quality safety and socio-economic environment. The frequent occurrence of "toxic cowpea" incidents is mainly due to the unscientific application of insecticides to control destructive bean flower thrips (BFT, *Megalurothrips usitatus*). The BFTs have developed significant resistance to different types of insecticides, including pyrethroids, diamides, neonicotinoids, etc., urgently requiring new insecticidal techniques to supplement or replace insecticides with high levels of resistance [2]. Sulfoxaflor (SUL), a nicotinic acetylcholine receptor agonist (nAChRs), is the first novel sulfoximine insecticide, which is effective against a variety of sucking pests [3]. Due to its unique chemical structure, SUL has been widely used to control sucking pests that have developed resistance to multiple currently-registered insecticides, including pyrethroids, neonicotinoids and carbamates [4, 5]. Additionally, because of its high efficacy, broad insecticidal spectrum and environmental safety, it is expected to become one of the mainstream insecticides for sucking pests in the future for a long time [6]. However, the latest monitoring results indicate that the BFTs in the Hainan province of China have developed resistance to SUL (65 fold), significantly higher than spinetoram (3.1–6.5 fold), emamectin benzoate (9.3–52 fold) and chlorfenapyr (2.5–16 fold), resulting in a gradual decline in the effectiveness of insecticides [2, 7]. Currently, the major method for thrip management is the combined or alternating use of different types of pesticides, but this is not a long-term solution [8]. Therefore, the development of novel eco-friendly agents to increase the susceptibility of BFTs to insecticides has become urgent to cope with the insecticide resistance.

The resistance mechanism of BFTs mainly includes the metabolic resistance caused by elevated detoxifying enzyme activity and target resistance caused by reduced sensitivity of target sites for insecticide action [9, 10]. SUL not only acts on insect nAChRs, but also affects monooxygenases (cytochrome P450 enzymes, CYPs) to consequently lead to resistance to SUL [3, 11]. Therefore, managing metabolic resistance is one of the effective ways to improve the sensitivity of pests to insecticides. Metabolic resistance is a complicated physiological process involving changes in enzyme activity due to the over expression of detoxification genes in insect pests. The famous detoxifying enzymes include cytochrome P450 enzymes (P450), glutathione S-transferases (GST), peroxidase (POD), superoxide dismutase (SOD), UDP-glucuronosyltransferases (UGTs) and ATP-binding cassette transporters (ABC transporters). These enzymes facilitate insects to degrade or transform insecticides, thereby reducing their toxicity [12, 13]. However, there are lots of detoxification genes, and achieving resistance management remains challenging due to the diversity of detoxification genes. In vertebrates, Nrf2 is a key transcription factor regulating antioxidant and detoxifying enzyme genes [14–16]. It participates in various biological processes such as redox balance, drug metabolism and excretion, energy metabolism, apoptosis, and aging [17]. Under normal physiological conditions, Nrf2 binds to the Kelch-like ECH-associated protein 1 (Keap1) in the cytoplasm, leading to its degradation. Whereas, under stress conditions, Nrf2 is translocated to the nucleus, and binds to the antioxidant response elements in the promoter regions of downstream detoxification genes, regulating their expression [18]. Therefore, Nrf2 is regarded as a good target for improving the sensitivity of insects to insecticides.

RNA biopesticides are polynucleotide preparations that can interfere with or inhibit the transcription of specific genes in target organisms [19]. Compared to traditional pesticides, RNA pesticides have various advantages such as strong specificity, lower development cost and eco-friendly [20, 21]. However, their field application faces technical bottlenecks such as the easy degradation of double-stranded RNA (dsRNA) by RNases, low delivery efficiency and high production cost of dsRNA, which limit the practical field application of RNA biopesticides [22]. In recent years, the rapid development of nanotechnology in agriculture has driven the continuous development of traditional agriculture in interdisciplinary fields [23]. Nanocarrier-enabled delivery system can protect dsRNA from degradation by ribonucleases, and achieve effective delivery of dsRNA by activating clathrin-mediated endocytosis [24–27]. Additionally, nanocarrier can spontaneously load insecticide into insecticide/nanocarrier complex with better properties, including nanoscale particle size, smaller contact angle, reduced surface tension, amplified contact area, enhanced plant uptake, etc., which promote the insecticidal activity while reducing the application amount [28–32]. Therefore, the application of nanocarrier co-loaded with dsRNA targeting *nrf2* and insecticide provides a novel method for increasing insecticide susceptibility.

Our team has established a star polycation (SPc)-based nano-delivery platform, which can not only assemble with dsRNA for strong stability and efficient delivery, but also load insecticides to increase their insecticidal activity [29, 33, 34]. Recently, our team has designed and synthesized a novel hydrophilic-lipophilic diblock polymer (HLDP), which can combine with various types of pesticides due to its rich functional groups [32]. Here, this study aimed to prepare a HLDP-based multicomponent

RNA nano-biopesticide with ds*Nrf2* and SUL to increase the susceptibility of destructive BFTs to insecticides. The regulatory role of *nrf2* in insecticide detoxification and metabolism was firstly demonstrated in BFTs via RNA interference (RNAi), RNA-seq analysis and enzyme activity assay. Then, the pET28-BL21 (DE3) RNase III-expression system was employed to synthesize ds*Nrf2* to construct a multicomponent RNA nano-biopesticide (SUL/HLDP/ds*Nrf2* complex), and its self-assembly mechanism, morphology and particle size were clarified via isothermal titration calorimetry (ITC), agarose gel retardation assay, ultra-performance liquid chromatography (UPLC), transmission electron microscopy (TEM) and dynamic light scattering (DLS). To explore the advantages of multicomponent RNA nano-biopesticide, its contact angle, contact area and retention were examined on cowpea leaves, and the plant uptake of both SUL and dsRNA was investigated. Furthermore, the delivery efficiency of multicomponent RNA nano-biopesticide was determined in vivo and in vitro. Finally, the insecticidal activity of multicomponent RNA nano-biopesticide was evaluated against BFTs in the laboratory and field, and the synergistic ratio was calculated. Overall, the current study demonstrated the regulatory role of *nrf2* in insecticide detoxification and metabolism, and designed a HLDP-based multicomponent RNA nano-biopesticide targeting *nrf2* to increase the susceptibility of destructive BFTs to insecticides.

Materials and methods

Insect rearing and cell culture

The adults of BFTs were collected in the cowpea field of the Sanya Institute of China Agricultural University, where no pesticides were applied. All stages of BFTs were reared on cowpea seedlings (*Vigna unguiculata*) and maintained at 26 ± 1 °C and 65% relative humidity under a 16 L: 8 D photoperiod. *Drosophila* S2 cells were cultured in Serum-Free Insect Cell Culture Medium (Thermo Fisher Scientific Inc., USA) at 25 °C.

Chemical reagents and HLDP synthesis

The SUL standard and commercial SUL (Active ingredient content: 50%) were bought from Shanghai Macklin Biochemical Technology Co., Ltd. (China) and Corteva agriscience (USA), respectively. The chemical reagents for the synthesis of HLDP included the ε-caprolactone (ε-CL), $Sn(Oct)_2$, one-butanol, 2-bromo-2-methylpropionyl bromide (BIBB), trimethylamine (TEA, 99%) and Sn $(Oct)_2$ purchased from Heowns BioChem Technologies (China), 2-(Dimethyl amino) ethyl methacrylate (DMAEMA, 99%) purchased from Energy Chemical (China), and tetrahydrofuran (THF), N,N,N′,N′,N″-Pentamethyl diethylenetriamine (PMDETA, 98%) and CuBr (99.999%) purchased from Sigma-Aldrich (USA). Other chemical reagents were obtained from Beijing Chemical Works (China).

The HLDP was synthesized according to the procedure described by Yin et al. [32]. One-butanol (100 mg, 1.35 mmol), ε-CL (6.16 g, 54 mmol) and Sn $(Oct)_2$ (310 mg) were incubated in an oil bath at 90 °C for 9 h. After the reaction was completed, dichloromethane (30 mL) was added, followed by the addition of cold methanol to precipitate a white solid powder of linear polycaprolactone PCL. PCL (3 g, 0.58 mmol) solution was added dropwise with BIBB (3 g, 13.04 mmol), THF (30 mL) and TEA (4 g, 40 mmol), and then cold methanol was added to terminate the reaction. The resulting precipitate was collected by filtration to obtain PCL-Br as a white powder. Finally, PCL-Br (100 mg, 0.04 mmol) was added to DMAEMA (0.87 g, 6.07 mmol), and dissolved in 2 mL of dry THF, followed by the addition of CuBr (15 mg, 0.1 mmol) and PMDETA (37 mg, 0.21 mmol). The reaction was carried out at 65 °C for 5 h, and after the reaction, dialysis and freeze-drying were performed to obtain HLDP as a white solid product.

RNA-seq analysis for exploring potential function of *nrf2*

RNAi technology and RNA-seq analysis were performed to examine the impact of *nrf2* on detoxification and metabolism in BFTs. The ds*Nrf2* was synthesized using the T7 RiboMAX Express RNAi System (Promega, USA). The specific steps were as follows: Thirty BFT adults were collected, and total RNA was extracted using the RNA Easy Fast Tissue/Cell Kit (TaKaRa, Japan). The 300 ng RNA was reverse-transcribed into cDNA using the PrimeScript™ RT Reagent Kit with gDNA Eraser (Perfect Real Time) (TaKaRa, Japan). Primers containing the T7 promoter sequence (Table S1) were used to amplify the gene fragments of *nrf2* and *enhanced green fluorescent protein* (*eGFP*), which were then cloned into the pMD19T-Vector (TaKaRa, Japan) and transformed into *Escherichia coli* DH5α strain (TSINGKE, China). Plasmids were extracted and verified by Sanger sequencing, followed by dsRNA synthesis using the T7 RiboMAX Express RNAi System (Promega, USA). The ds*eGFP* was used as a control in the current study.

To prepare the ds*Nrf2*/HLDP complex, the optimal mass ratio of ds*Nrf2* and HLDP was firstly examined using the agarose gel retardation assay. One μg of ds*Nrf2* was incubated with HLDP at the mass ratios of 1:0, 1:1, 1:2, 1:3, 1:4 and 1:5 at room temperature for 15 min, and the mixture was analyzed using the agarose gel electrophoresis. In the subsequent experiments, the ds*Nrf2*/HLDP complex was prepared at the optimal mass ratio of 1:4. For RNAi experiments, the cowpea was cut into 3 cm segments, and 10 μL solutions of ds*Nrf2*/HLDP complex (600: 2400 ng/μL), ds*eGFP*/HLDP complex (600: 2400 ng/μL), ds*Nrf2* (600 ng/μL) and ds*eGFP* (600 ng/μL)

were individually applied to the segment. These segments were used to feed BFT adults for 24 h in ventilated centrifuge tubes, and the total RNA of BFTs was extracted and used to transcribe into cDNA. The expression levels of *nrf2* were examined using the quantitative real-time PCR (qRT-PCR) with the primers listed in Table S1. The qRT-PCR was performed with the Step One Plus Real-Time PCR system (Applied Biosystems, USA) using the SuperReal PreMix Plus (SYBR Green) (Tiangen Biotech, China). The relative mRNA level of *nrf2* was determined using the $2^{-\Delta\Delta CT}$ method with *RPL* (GenBank accession: XM_026436599) as the internal reference gene [35]. Each treatment included three independent samples, with each sample consisting of 30 BFT adults.

For RNA-seq analysis, the total RNA of BFT adults treated with ds*Nrf2*/HLDP complex or ds*eGFP*/HLDP complex was extracted. Then, the RNA-seq analysis was carried out by Novogene Co., Ltd. (China) according to the standard protocol. Above total RNA was used to construct RNA sequencing libraries using the NEBNext® Ultra™ RNA Library Prep Kit for Illumina® (NEB, Beverly), and the sequencing was performed on the Illumina Novaseq 6000 platform. The expression levels of various genes were determined using the number of Fragments Per Kilobase of transcript per Million fragments mapped (FPKM) [36]. Differentially expressed genes (DEGs) were identified with $P \leq 0.05$ and $|\log2 \text{ (fold change)}| \geq 1$. The volcano plot visually displayed the distribution of DEGs for each comparison group. Kyoto Encyclopedia of Genes and Genomes (KEGG) was used to analyze the enrichment of DEGs [37]. The heatmaps were based on the correlation coefficients calculated from FPKM values. The DEG set was created by taking the union of differential genes from the comparison groups, providing an intuitive visualization of both inter-group sample differences and intra-group sample replicates [38]. Each treatment was conducted with three independent replicates.

Effect evaluation of *nrf2* RNAi on detoxification gene expression and enzyme activity

The RNA-seq results indicated that the *nrf2* regulated the resistance of BFTs against insecticides. To clarify the impact of *nrf2* RNAi on detoxification gene expression, the BFT adults were treated with ds*Nrf2*/HLDP complex and ds*eGFP*/HLDP complex following the method described above. Total RNA was extracted at 24 h after the oral feeding, and the expression levels of detoxification genes such as *P450s*, *GSTs*, *PODs* and *SODs* were examined using the qRT-PCR. Each treatment included three independent samples, with each sample containing 30 BFT adults. Subsequently, the activities of detoxification enzymes were examined in above treated BFT adults. The 0.1 g sample of adults was homogenized in 1 mL of extraction solution to prepare the crude enzyme solution (Suzhou Comin Biotechnology, China). The activities of P450, GST, POD and SOD were measured using the micro-method according to the procedures of assay kits (Suzhou Comin Biotechnology, China). The total protein content of enzyme source was quantified using the BCA protein assay kit (Beijing BioDee Biotechnology, China). Each experiment was repeated three times.

Loading capacity assay of HLDP for SUL

To prepare the SUL/HLDP complex, the loading capacity of HLDP toward SUL was determined using the UV spectrophotometry method. The SUL standard was dissolved in ddH_2O to prepare a storage solution (2 mg/mL). This storage solution was then diluted with ddH_2O to prepare a series of dilutions at the concentrations of 0, 3, 6, 9, 12 and 15 μg/mL. The absorbance of these solutions was measured using the ultraviolet-visible (UV−vis) spectrophotometry (PHILES, China) in the wavelength range of 230 to 350 nm. A standard curve was then constructed based on the OD values at 251 nm. Then, excess SUL (2.5 mL, 2 mg/mL) was incubated with HLDP (2.5 mL, 1 mg/mL) at room temperature for 15 min, and the mixture was placed in a dialysis bag with a molecular weight cut-off of 3400 Da (Solarbio Life Sciences, China), which was immersed in 1000 mL ddH_2O for 12 h. Absorbance was measured at 251 nm, and SUL concentration was calculated based on the standard curve. The pesticide-loading content (PLC) was calculated as PLC (%) = weight of SUL loaded in complex ÷ weight of SUL/HLDP complex × 100. In the subsequent experiments, SUL/HLDP complex was prepared based on the PLC.

Synthesis of ds*Nrf2* in vivo

The ds*Nrf2* was efficiently synthesized using the engineered bacteria BL21 (DE3) RNase III- according to the previously-described method [39]. Specific primers with restriction sites were designed based on the sequence of *nrf2* (Table S1), and the target sequence was obtained through PCR cloning. This sequence was then ligated into the pET28a(+) expression vector via double digestion, which was subsequently transformed into the BL21 (DE3) RNase III- strain to construct the pET28-BL21 (DE3) RNase III- expression system and incubated at 37℃ overnight. A single colony was selected and cultured in 10 mL of LB liquid medium containing 100 mg/L kanamycin (Kan) with shaking overnight at 37 °C. When the $OD_{600\ nm}$ value reached 0.4, isopropyl β-D-1-thiogalactopyranoside (IPTG) (1 mM) was added to induce the expression of ds*Nrf2*. Lysozyme was then added to the medium to the final concentration of 1.3 mg/mL to disrupt the cell wall, and the mixture was kept at 75 °C for 5 min to inactivate the bacteria. The obtained bacterial solution contained ds*Nrf2*.

Assembly mechanism analysis of SUL/HLDP/ds*Nrf2* complex

As a widely adopted method, the ITC was employed to measure the primary interaction force between SUL and HLDP [40]. In the Nano ITC (TA Instruments Waters, USA), 0.05 mM SUL was titrated with 0.5 mM HLDP. After completion, each titration peak was integrated using the Origin7 software (OriginLab Co., USA). The experiment was conducted at 25 °C, and the ΔG was calculated using the formula ΔG = ΔH - TΔS. To further elucidate the assembly mechanism of SUL/HLDP complex with ds*Nrf2*, 0.0414 μM SUL/HLDP complex was titrated with 0.3 μM ds*Nrf2*, and the thermodynamic parameters were recorded similarly as above. Furthermore, one μg of ds*Nrf2* was incubated with the SUL/HLDP complex at the mass ratios of 1:0, 1:1, 1:2, 1:3, 1:4, 1:5 and 1:6 (ds*Nrf2*: HLDP) for 15 min, and the mixture was tested using the agarose gel retardation assay.

To quantify the SUL in SUL/HLDP/ds*Nrf2* complex, SUL/HLDP/ds*Nrf2* complex was dialyzed in ddH_2O for 12 h similarly as above. The concentration of SUL outside the dialysis bag was quantified using the ACQUITY UPLC H-Class (Waters, USA). The UPLC column was BEH C18 (2.1 × 100 mm, 1.7 μm), with a column temperature of 40 °C. The mobile phase consisted of acetonitrile and 0.1% formic acid aqueous solution. The injection volume was 10 μL, and the detection wavelength was 260 nm. A standard curve was constructed based on the chromatographic data of SUL dilutions (0, 20, 40, 100, 120, 160 and 200 μg/mL) to calculate the quality of SUL in the SUL/HLDP/ds*Nrf2* complex. The optimal mass ratio for the preparation of SUL/HLDP/ds*Nrf2* complex was 14:69:17, which was adopted to prepare SUL/HLDP/ds*Nrf2* complex in the following experiments.

Particle size and morphology examination of SUL/HLDP/ds*Nrf2* complex

The particle sizes and zeta potentials of SUL (1 mg/mL), SUL/HLDP complex (SUL concentration: 1 mg/mL), ds*Nrf2*/HLDP complex (HLDP: ds*Nrf2* = 4: 1) and SUL/HLDP/ds*Nrf2* complex (SUL concentration: 1 mg/mL) were measured using the Particle Sizer and Zeta Potential Analyser (Anton Paar, Austria). Each treatment included three independent samples. For each sample, 5 μL of solution was placed on a copper grid, air-dried, and then observed for morphological characteristics using a transmission electron microscope (TEM) (JEOL-F200, Japan).

The Tindall effect was the optical scattering phenomenon of particles in suspension or colloidal systems. When the colloidal solution was irradiated with light of a certain wavelength, a bright light path can form in liquid or gas systems, reflecting whether the test liquid has undergone nano-level aggregation [41]. The 40 mL solutions of HLDP (based on the PCL toward SUL), SUL (0.1 mg/mL) and SUL/HLDP/ds*Nrf2* complex (SUL concentration: 0.1 mg/mL) were separately prepared. A red laser pointer (wavelength 650 nm) was used for irradiation, and photographs were taken in the dark using a Canon EOS R6 Mark II camera (Canon, Japan).

Contact angle, contact area and surface tension analysis of SUL/HLDP/ds*Nrf2* complex

The formulations of SUL/HLDP/ds*Nrf2* complex (SUL concentration: 0.1 mg/mL), ds*Nrf2* (based on the optimal binding mass ratio of HLDP to ds*Nrf2*), SUL (0.1 mg/mL), HLDP (based on the PCL of SUL) and ddH_2O were separately dropped onto cowpea leaves. After the droplets stabilized for 20 s, observation and measurement were carried out using a contact angle measuring instrument (DataPhysics OCA25A, Germany), and the contact angle of droplet image was calculated using an ellipse fitting algorithm. Each solution was tested three times. Meanwhile, photographs were taken using a microscopic operation system (Nikon, Japan), and the contact areas of tested solutions dropped onto cowpea leaves and glass slides were statistically analyzed using the ImageJ 1.8 (National Institutes of Health, USA). Each treatment included three independent samples.

Surface tension analysis was performed using a DCAT 21 surface tensiometer based on the Wilhelmy plate method [42]. Measurements were taken at 298 ± 0.1 K for ddH_2O, HLDP (based on the PCL of SUL), SUL (0.1 mg/mL), ds*Nrf2* (based on the optimal mass ratio of HLDP to ds*Nrf2*) and SUL/HLDP/ds*Nrf2* complex (SUL concentration: 0.1 mg/mL) solutions. The tensiometer was calibrated using the surface tension of water, ensuring the cleanliness of plate and glassware. During the measurement of samples, it was ensured that the surface tension values remained constant, indicating that equilibrium had been reached. Each sample was measured three times consecutively, with a standard deviation not exceeding ± 0.20 mN/m.

Retention, plant uptake and leaf adhesion assay of SUL/HLDP/ds*Nrf2* complex

The retention of SUL/HLDP/ds*Nrf2* complex on cowpea leaves was measured using the weighing method. First, the initial weight (M1) of cowpea leaves (1.8 cm^2) was measured. Then, the leaves were immersed in SUL (100 mg/L) and SUL/HLDP/ds*Nrf2* complex (SUL concentration of 100 mg/L) solutions for 1 min, respectively. After removing the leaves, they were suspended in the air until no droplets naturally fell off, and their weight (M2) was recorded. The retention was calculated using the formula: retention (mg/cm^2) = (M2 - M1) ÷ leaf area. Each treatment included three independent samples.

The plant uptake of SUL/HLDP/ds*Nrf2* complex was examined using the UPLC. The four-leaf stage seedlings

of oil rapes at the same growth stage were carefully washed with ddH_2O and air-dried. Subsequently, the seedlings were immersed in SUL (0.2 mg/mL) and SUL/HLDP/ds*Nrf2* complex (SUL concentration: 0.2 mg/mL) solutions for 1 min, respectively. The residual SUL on the seedling surface was thoroughly washed with ddH_2O at 6 h after the immersion. The 200 mg of seedlings was added to 20 mL of acetonitrile and 3 g of sodium chloride. The mixture was homogenized using an electric grinder, followed by centrifugation at 10,000 r/min for 10 min, and the supernatant was collected. Subsequently, the 10 mL supernatant was evaporated to near dryness under nitrogen gas at 40 °C. The 6 mL of methanol-dichloromethane (5:95, v: v) was added and vortexed for 2 min. The solution was purified using an amino column (BKMAM, China), and the eluate was evaporated under nitrogen gas at 40 °C. Finally, 2 mL of methanol: water (1:1, v: v) was added, vortexed for 2 min, and filtered through a 0.22 μm organic membrane. The SUL concentration was quantified using the UPLC. Specific UPLC conditions are described above. Each treatment included three independent samples.

To facilitate the observation for plant uptake, fluorescent ds*eGFP* was synthesized using the Fluorescein RNA Labeling Mix Kit (Roche Diagnostics, Germany) to prepare the SUL/HLDP/ds*eGFP* complex (ds*eGFP*: 1 μg). Simultaneously, SUL/HLDP complex (0.808:4 μg) and ds*eGFP* (1 μg) were prepared as controls. The bean seedlings were cultured in the above solutions for 6 h, and the roots were washed by water. The root uptake of fluorescent ds*eGFP* was determined using the fluorescent inverted microscope (LEICA, Germany).

The biological scanning electron microscope (SEM) was employed to observe the adhesion of SUL/HLDP/ds*eGFP* complex on cowpea leaves. For the preparation of biological SEM samples, cowpea leaves were soaked in ddH_2O, SUL (0.2 mg/mL) and SUL/HLDP/ds*Nrf2* complex (SUL concentration: 0.2 mg/mL) solutions for 1 min, respectively. After natural air drying, the leaves were soaked in fixative solution (glutaraldehyde, 2.5%, pH = 7.4) at room temperature for 4 h, dehydrated with gradient concentration ethanol (30%, 50%, 70%, 80%, 90%, 95%, 100%) for 15 min respectively, then dried with critical point dryer (Leica EM CPD300, Germany), sputter-coated with gold, and photographed using the SEM (JCM-7000 NeoScope™, Japan).

Delivery efficiency assay of SUL/HLDP/ds*Nrf2* complex in vivo and in vitro

The fluorescent ds*eGFP* was applied to prepare the SUL/HLDP/ds*eGFP* complex to assess its delivery efficiency in BFT adults (in vivo) and *Drosophila* S2 cells (in vitro). The 0.2 μL solutions of SUL/HLDP complex (0.808:4 μg), ds*eGFP* (1 μg) and SUL/HLDP/ds*eGFP* complex (ds*eGFP*: 1 μg) were individually applied on the notum of BFT adults, and the adults were washed by ddH_2O at 6 h after the topical application. Photographs were taken using a fluorescence inverted microscope (LEICA, Germany), and fluorescence intensity was quantified using the ImageJ 1.8 (National Institutes of Health, USA). Each treatment included three biological replicates.

The *Drosophila* S2 cells were cultured to a density of 5×10^5/mL, then the SUL/HLDP complex (0.808:4 μg), ds*eGFP* (1 μg) and SUL/HLDP/ds*eGFP* complex (ds*eGFP*: 1 μg) were individually added to 0.5 mL of fresh cell culture medium. The 0.4 mL of fresh medium was used to replace the cell culture medium at 6 and 12 h after the incubation. The mixture was gently pipetted and then dropped onto slides treated with ConA. The cells were fixed with 4% paraformaldehyde (PFA) for 20 min and washed three times with 1 mL PBS. The cells were sealed with DAPI sealing solution (Solarbio Life Sciences, China), and the fluorescence was detected using a confocal microscope (Leica SP8, Germany). Fluorescence intensity was quantified using the ImageJ 1.8 (National Institutes of Health, USA). Each treatment included three independent samples.

Bioactivity assay of SUL/HLDP/ds*Nrf2* complex toward BFTs in the laboratory

The commercial SUL was used to determine the median lethal concentration (LC_{50}) value for BFT adults. Cowpea segments (3 cm) were immersed in various SUL solutions at the concentrations of 0, 0.1, 0.2, 0.4, 0.8, 1.6 and 3.2 mg/mL for 1 min, and the BFT adults were also immersed in above solutions for 30 s. After air-drying, the cowpea segments were used to feed 30 BFT adults in ventilated centrifuge tubes, and mortality was recorded at 48 h after the oral feeding. The LC_{50} value was calculated using the SPSS software (version 23.0, USA), and the experiment was repeated three times.

Based on the LC_{50} value of commercial SUL (Actual content of SUL: 0.177 mg/mL), the following solutions were prepared: SUL (0.177 mg/mL), SUL/HLDP complex (0.177:0.876 mg/mL), SUL/HLDP/ds*eGFP* complex (0.177:0.876:0.219 mg/mL), SUL/HLDP/ds*Nrf2* complex (0.177:0.876:0.219 mg/mL), ds*eGFP* (0.219 mg/mL), ds*Nrf2* (0.219 mg/mL), ds*eGFP*/HLDP complex (0.219:0.876 mg/mL) and ds*Nrf2*/HLDP complex (0.219:0.876 mg/mL). The same immersion method and oral feeding as described above were used to determine the BFT mortalities at 12, 24, 36 and 48 h after the treatment. The synergistic effect of insecticidal activity was evaluated using the formula: normalized synergistic ratio = mortality of adults treated with the each formulation ÷ average mortality of adults treated with SUL alone. The experiment was conducted in three replicates, with 30 adults per replicate. Additionally, the expression levels

of *nrf2* were detected at 12, 24, 36 and 48 h after the treatment with SUL/ds*eGFP* complex (0.177:0.219 mg/mL), SUL/ds*Nrf2* complex (0.177:0.219 mg/mL), SUL/HLDP/ds*eGFP* complex (0.177:0.876:0.219 mg/mL) and SUL/HLDP/ds*Nrf2* complex (0.177:0.876:0.219 mg/mL), and the expression levels of detoxification genes (*P450*, *GST*, *POD* and *SOD*) were detected at 48 h after the treatment. Each treatment included three independent samples.

Control efficacy assay of SUL/HLDP/ds*Nrf2* complex in the field

Based on the LC_{50} value of commercial SUL (Actual content of SUL: 0.177 mg/mL), the control efficacy of SUL/HLDP/ds*Nrf2* complex was evaluated in the cowpea field of the Sanya Institute of China Agricultural University (Actual content of SUL: 0.177 mg/mL) and Sanya Institute of Breeding and Multiplication, Hainan University (Actual content of SUL: 0.124 mg/mL), respectively. The row spacing of cowpea seedlings was 0.5 m, and the plant spacing within the row was 0.2 m. The population density of BFT adults on cowpea flowers was about 30 per flower. From 7 to 9 a.m. (when cowpea petals were open), a 528B electric sprayer (Shenzhen Lange Technology Co., Ltd., China) was used to spray HLDP (0.876 mg/mL), ds*Nrf2*/HLDP complex (0.219:0.876 mg/mL), SUL (0.177 mg/mL), SUL/HLDP complex (0.177:0.876 mg/mL) and SUL/HLDP/ds*Nrf2* complex (0.177:0.876:0.219 mg/mL) at the dose of 100 mL/m² in the cowpea field of the Sanya Institute of China Agricultural University, and HLDP (0.614 mg/mL), ds*Nrf2*/HLDP complex (0.153:0.614 mg/mL), SUL (0.124 mg/mL), SUL/HLDP complex (0.124:0.614 mg/mL) and SUL/HLDP/ds*Nrf2* complex (0.124:0.614:0.153 mg/mL) at the dose of 100 mL/m² in the cowpea field of the Sanya Institute of Breeding and Multiplication, Hainan University. The ddH_2O was sprayed as a negative control. Each plot was about 20 m^2, containing 40–60 plants. Ten plants were selected from each plot as ten replicates, and the number of thrips on the flowers was recorded at 0, 1, 3, 5 and 7 d after the treatment. The dropping rate of insect and control efficacy were calculated using the following formulas.

Dropping rate of insect (%) = (number of pest before pesticide application - number of pest after pesticide application) ÷ number of pest before pesticide application × 100.

Control efficacy (%) = (dropping rate of insect in the treatment plot - dropping rate of insect in the control plot) ÷ (100 - dropping rate of insect in the control plot) × 100.

Statistical analysis

Graph generation and statistical analysis were performed using the GraphPad Prism 8 and IBM SPSS Statistics software (Version 22), respectively. Significant difference between two groups or multiple-comparison analysis was determined using the independent *t*-test or Duncan's multiple range test at $P < 0.05$ significance level. The descriptive data are shown as the mean and standard errors of mean.

Results

Crucial regulatory role of *nrf2* in the expression of detoxification genes

The ds*Nrf2* was synthesized to down-regulate *nrf2* expression via nanocarrier-mediated RNAi. The optimal mass ratio of ds*Nrf2* to HLDP was examined, and ds*Nrf2* band disappeared when the mass ratio was 1:4, indicating that ds*Nrf2* could be fully loaded by HLDP at this mass ratio (Fig. 1a). Thus, the ds*Nrf2*/HLDP complex was prepared according to the mass ratio of 1:4 in the subsequent experiments. Then, the BFT adults were treated with the ds*Nrf2*/HLDP complex via oral feeding, and the RNAi efficiency was determined using the qRT-PCR (Fig. 1b). The results showed that the expression of *nrf2* in the BFT adults treated with the ds*Nrf2*/HLDP complex decreased by 61.87% compared to ds*Nrf2* alone (Fig. 1c). Subsequently, the transcriptome samples were tested, and the correlation of each biological replicate and sequencing quality were high enough for the RNA-seq analysis (Fig. S1, Table S2). After *nrf2* RNAi in BFT adults, volcano plot analysis identified 867 down-regulated genes and 1125 up-regulated genes (Fig. 1d). KEGG analysis showed that DEGs were enriched in various metabolism pathways, such as starch and sucrose metabolism, carbon metabolism, fatty acid metabolism, pyrimidine metabolism, drug metabolism-other enzymes, etc. (Fig. 1e). GO enrichment also supported these findings that the DEGs were mainly related with insecticide metabolic resistance, including oxidation-reduction process, oxidoreductase activity and drug metabolic process (Fig. S2). Heatmap analysis showed that the expression of key detoxification genes (*P450s*, *GSTs*, *PODs* and *SODs*) was significantly inhibited after *nrf2* RNAi (Fig. 1f), and the FPKM values were also significantly reduced (Fig. 1g). The qRT-PCR results further demonstrated that the related detoxification genes were significantly suppressed after *nrf2* RNAi (Fig. 2a). Additionally, the suppression of *nrf2* expression significantly reduced the enzyme activities of P450s, GSTs, PODs and SODs from 5.93 to 3.34 nmol/min/mg prot, from 5.12 to 3.20 nmol/min/mg prot, from 4.04 to 2.27 U/mg prot and from 1.71 to 0.69 U/mg prot, respectively (Fig. 2b).

Self-assembly mechanism and quantitative analysis of SUL/HLDP/ds*Nrf2* complex

The *nrf2* fragment was constructed into the pET28a (+) vector and transformed into the BL21 (DE3) RNase III-strain to produce the ds*Nrf2* (Fig. 3a). Then, the HLDP

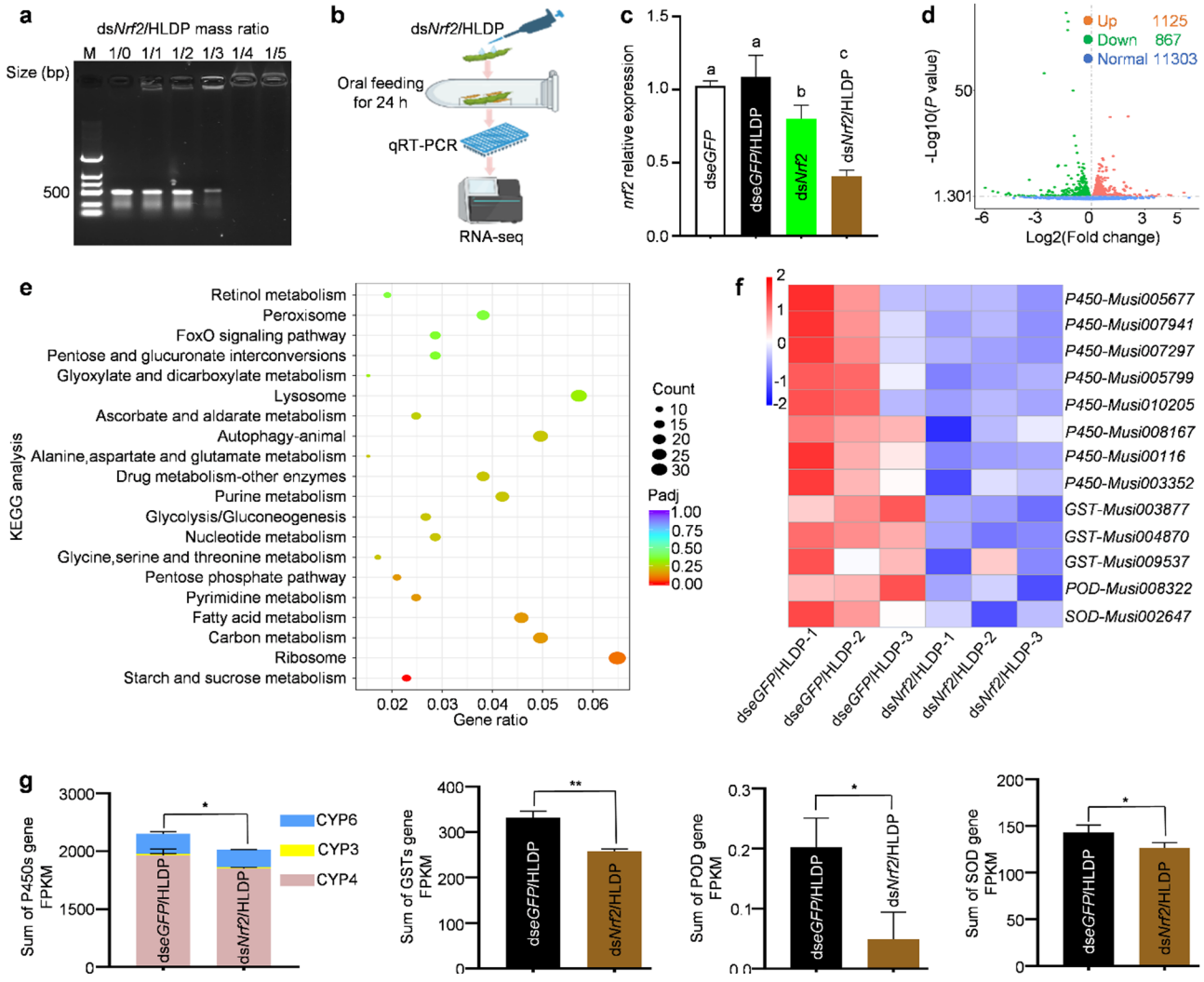

Fig. 1 RNA-seq analysis of the regulatory role of *nrf2* in detoxification genes. **(a)** Gel electrophoresis assay of ds*Nrf2* retardation by HLDP. One μg ds*Nrf2* was mixed with HLDP at various mass ratios. M: DNA marker. **(b)** Schematic diagram for RNA-seq analysis using the BFT adults treated with ds*Nrf2*/HLDP complex. **(c)** RNAi efficiency of ds*Nrf2*/HLDP complex at 24 h after the oral feeding. The ds*Nrf2* was mixed with HLDP at the mass ratio of 1:4. The gene expression was normalized to *RPL* gene. The experiment was repeated 3 times. Different letters above the bars indicate significant differences at $P < 0.05$ as determined by Duncan's multiple range test. **(d)** Analysis of DEGs with a volcano plot. Up- and down-regulated genes are represented by red and green dots, respectively. **(e)** KEGG enrichment of DEGs. **(f)** Heatmap analysis of various detoxification genes. Highly and lowly expressed genes are labeled as red and blue, respectively. **(g)** Sum of *P450s*, *GSTs*, *PODs* and *SODs* gene FPKM. P450s genes were divided into 3 subfamilies. Each treatment included three independent samples. The "*" and "**" indicate significant differences according to the independent *t*-test, respectively ($P < 0.05$ and $P < 0.01$)

was applied to assemble SUL and ds*Nrf2* simultaneously to prepare the SUL/HLDP/ds*Nrf2* complex. A standard curve of SUL was constructed using the UV spectrophotometry, and the PLC of HLDP was calculated to be 20.2% toward SUL (Fig. S3). The ITC was used to detect the interaction force between HLDP and SUL (Fig. 3b). According to the previous interpretation of ITC data [43], a high affinity constant (Ka) and a low dissociation constant (Kd) indicated an effective and strong interaction between HLDP and SUL, and this interaction was spontaneous due to the negative ΔG of -41.175 kJ/mol. The negative values of ΔH (-119 kJ/mol) and ΔS (-311.3 kJ/mol) suggested that the SUL/HLDP complex self-assembled through hydrogen bonds and Van der Waals forces.

Then, the agarose gel retardation experiment was conducted to further investigate the assembly of ds*Nrf2* with SUL/HLDP complex. The results showed that the band intensity of the migrated ds*Nrf2* gradually disappeared as the mass ratio decreased, indicating that the electrostatic interaction played an important role in the self-assembly process of the SUL/HLDP/ds*Nrf2* complex (Fig. 3c). Additionally, the ITC data suggested that the hydrogen bonds and Van der Waals forces also played important roles in the binding process of SUL/HLDP complex with ds*Nrf2* (Fig. 3d). As shown in Fig. 3c, the complexation

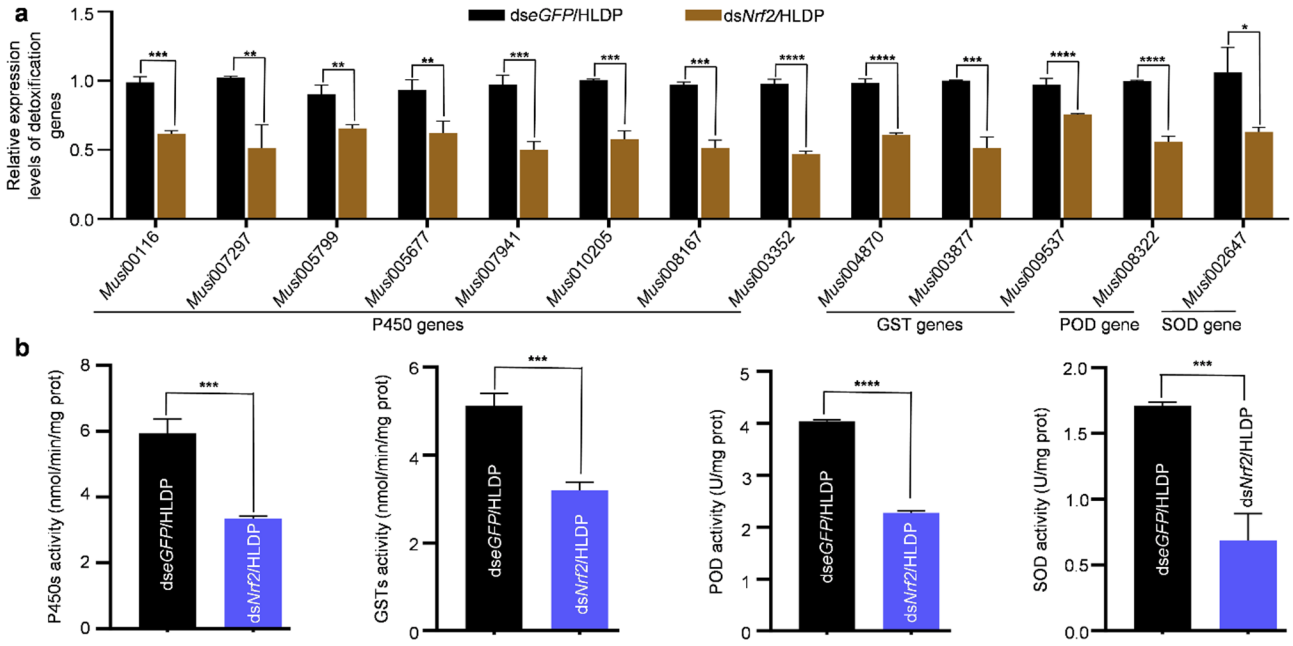

Fig. 2 Crucial regulatory role of *nrf2* in the expression of detoxification genes and enzyme activity. **(a)** Expression levels of various detoxification genes such as *P450s*, *GSTs*, *PODs* and *SODs* in BFT adults treated with ds*Nrf2*/HLDP complex through oral feeding. Each treatment included three independent samples. **(b)** Activities of detoxification enzymes in BFT adults treated with ds*Nrf2*/HLDP complex. Each treatment included three independent samples. The "*", "**", "***" and "****" indicate significant differences according to the independent *t*-test, respectively ($P < 0.05$, $P < 0.01$, $P < 0.001$ and $P < 0.0001$)

with HLDP increased the zeta potential of SUL from −5.31 mV to 28.38 mV, but the SUL/HLDP/ds*Nrf2* complex was negatively-charged (-0.2 mV), which was due to complexation with the negatively-charged ds*Nrf2*. To further quantify the SUL in the SUL/HLDP/ds*Nrf2* complex, the SUL/HLDP complex was incubated with ds*Nrf2* at the mass ratio of 4:1 (HLDP: ds*Nrf2*) and dialyzed for 12 h. The concentration of SUL outside the dialysis bag was quantified using the UPLC based on the standard curve (Fig. S4). The mass ratio of SUL: HLDP: ds*Nrf2* was calculated to be 14:69:17, indicating that the binding of SUL/HLDP complex with ds*Nrf2* had a negligible effect on the SUL loaded in HLDP.

Nanoscale particle size of SUL/HLDP/ds*Nrf2* complex

The morphology and particle size of SUL/HLDP/ds*Nrf2* complex were examined using the TEM and DLS, respectively. From several representative TEM images, it was observed that most SUL/HLDP/ds*Nrf2* complex consisted of nearly spherical particles with much smaller sizes compared to SUL alone (Fig. 4). The particle sizes of SUL, SUL/HLDP complex, ds*Nrf2*/HLDP complex and SUL/HLDP/ds*Nrf2* complex were 821.09, 140.30, 241.35 and 221.52 nm, respectively. The complexation with HLDP remarkably decreased the particle size of SUL, and the particle size of SUL/HLDP/ds*Nrf2* complex was slightly larger than that of SUL/HLDP complex, which might be due to the electrostatic adhesion of ds*Nrf2* on the surface of SUL/HLDP complex. The Tindall effect is a commonly used physical method to distinguish colloids from solutions, reflecting whether the liquid has undergone nanoscale aggregation. In the current study, a red laser was used to detect HLDP, SUL and SUL/HLDP/ds*Nrf2* complex, and the results revealed that, except for SUL, both HLDP and SUL/HLDP/ds*Nrf2* complex exhibited the Tindall effect, indicating that these two solutions were at the nanoscale (Fig. 5a).

Excellent adhesion and uptake performance of SUL/HLDP/ds*Nrf2* complex

The contact angle, surface tension and contact area of pesticide droplets reflect their spreading, deposition and adhesion on leaves, which are important factors influencing the control efficacy of pesticides. In the current study, the contact angle of SUL/HLDP/ds*Nrf2* complex on cowpea leaves (32.72°) was significantly smaller than those of ddH_2O (81.36°), HLDP (59.23°), SUL (66.01°) and ds*Nrf2* (54.97°) (Fig. 5b). Additionally, the surface tension of SUL/HLDP/ds*Nrf2* complex (44.18 mN/m) was also the smallest among those of ddH_2O (72.27 mN/m), HLDP (49.41 mN/m), SUL (63.74 mN/m) and ds*Nrf2* (66.25 mN/m) (Fig. 5c). Due to the smaller contact angle and surface tension, the contact area of SUL/HLDP/ds*Nrf2* complex was the largest on cowpea leaves among tested solutions (Fig. 5d), and the same phenomenon was observed on the glass slides (Fig. S5).

The retention of SUL and SUL/HLDP/ds*Nrf2* complex on the cowpea leaves were 0.83 and 1.96 mg/cm^2,

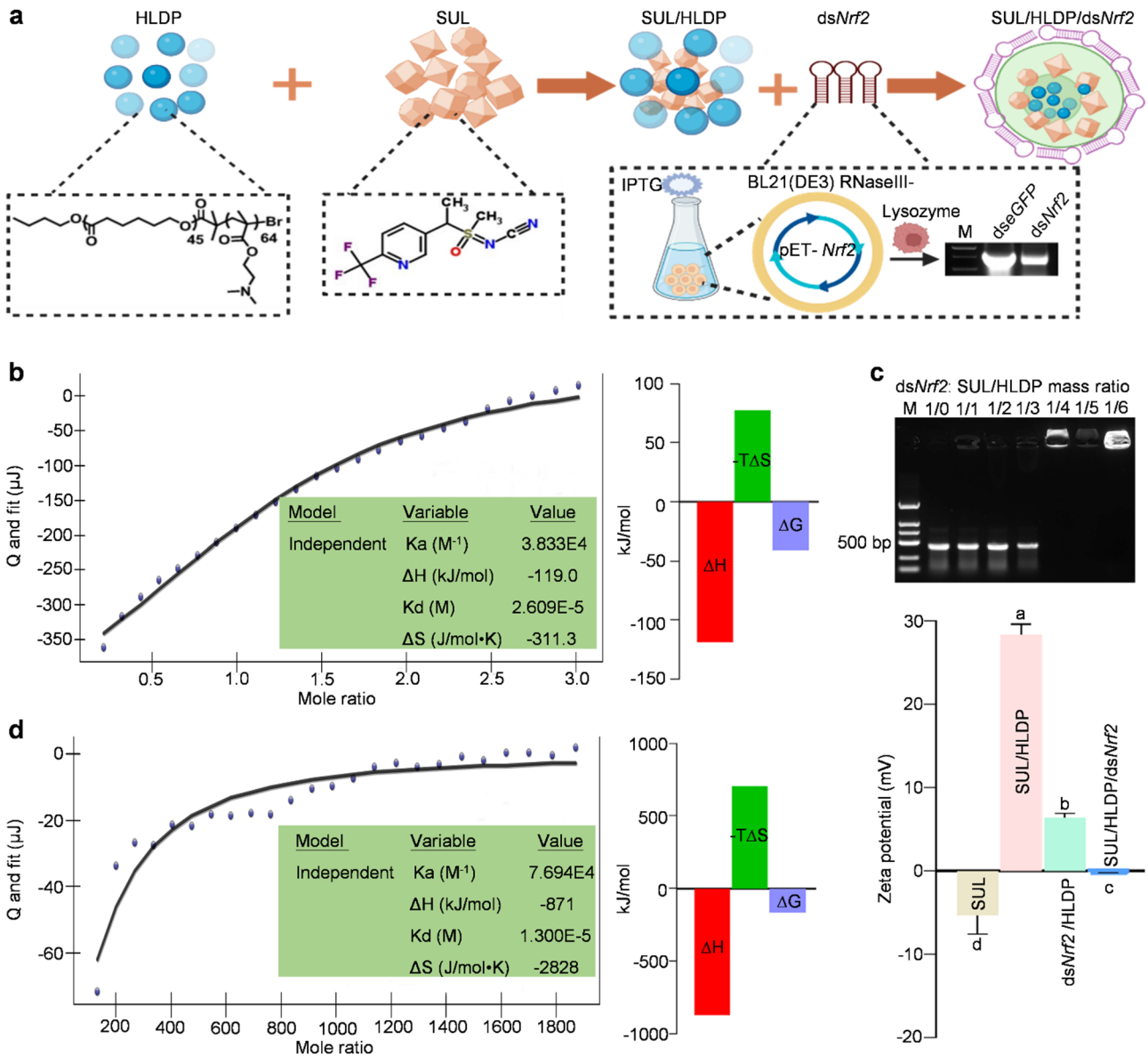

Fig. 3 Self-assembly mechanism of SUL/HLDP/ds*Nrf2* complex. **(a)** Schematic illustration of self-assembled SUL/HLDP/ds*Nrf2* complex. The HLDP assembled with SUL into SUL/HLDP complex, which further assembled with ds*Nrf2* expressed in pET28-BL21 (DE3) RNase III- expression system. **(b)** ITC titration of HLDP solution (0.5 mM) into SUL solution (0.05 mM). The test temperature was 25 °C, and ΔG was calculated using the formula ΔG = ΔH – TΔS. **(c)** Gel electrophoresis assay of ds*Nrf2* retardation by SUL/HLDP complex. One μg ds*Nrf2* was mixed with HLDP at various mass ratios. M: DNA marker. The zeta potentials of various formulations (SUL concentration: 1 mg/mL) at 25 ℃. Each treatment included three independent samples. Different letters above the bars indicate significant differences at $P < 0.05$ as determined by Duncan's multiple range test. **(d)** ITC titration of ds*Nrf2* solution (0.3 μM) into SUL/HLDP complex solution (0.0414 μM)

respectively (Fig. 5e). Compared to SUL alone, the retention of SUL/HLDP/ds*Nrf2* complex increased by 2.36 times. Additionally, the SUL concentrations in the plants treated with SUL alone and SUL/HLDP/ds*Nrf2* complex were 1.42 and 3.59 μg/mg, respectively, and the plant uptake of SUL was remarkably increased by 2.53 times with the aid of HLDP (Fig. 5f). To further explore the plant uptake of dsRNA, fluorescent ds*eGFP* was adopted to prepare the SUL/HLDP/ ds*eGFP* complex, and plant root was immersed in this solution to trace the ds*eGFP*. The fluorescence intensity of roots treated with SUL/HLDP/ds*eGFP* complex was stronger than those treated with fluorescent ds*eGFP* alone (Fig. 5g). Additionally, as shown in Fig. S6, the biological SEM results also indicated that the SUL/HLDP/ds*eGFP* complex was uniformly distributed on cowpea leaves, and its adhesion level was obviously higher than SUL alone. The above results indicated that the SUL/HLDP/ds*Nrf2* complex diffused more easily and had a strong affinity with the

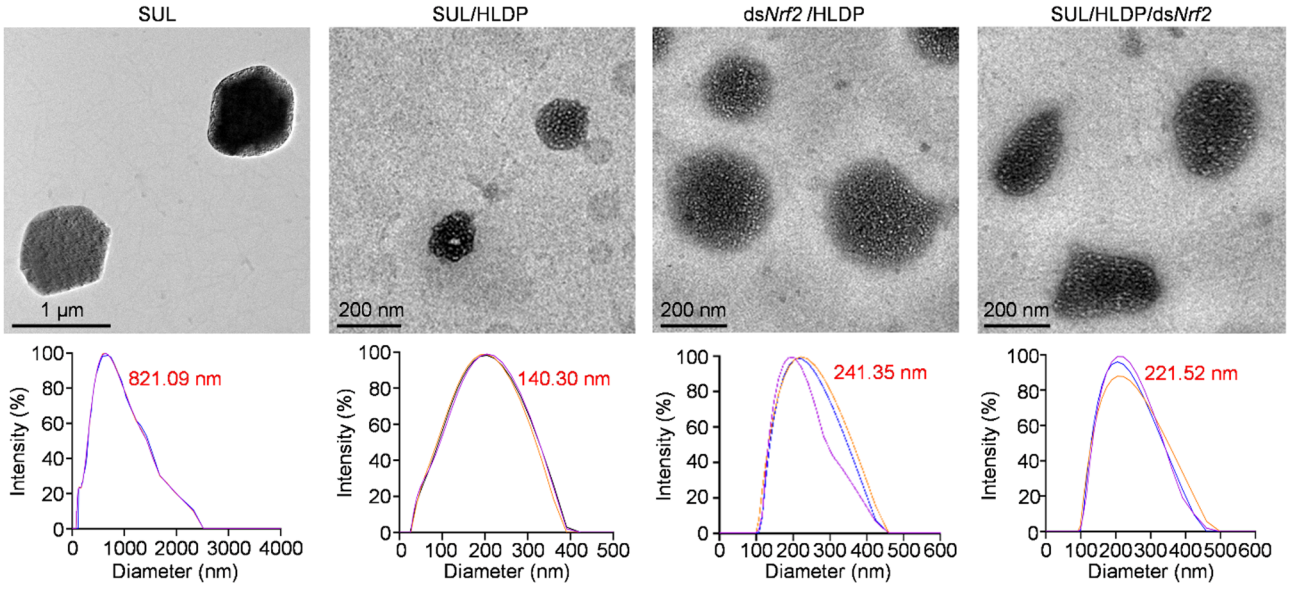

Fig. 4 Particle size and morphology of SUL/HLDP/ds*Nrf2* complex. TEM images and particle size distributions of various formulations. Each treatment was consisted of three independent samples. The numbers in red indicate the average particle sizes

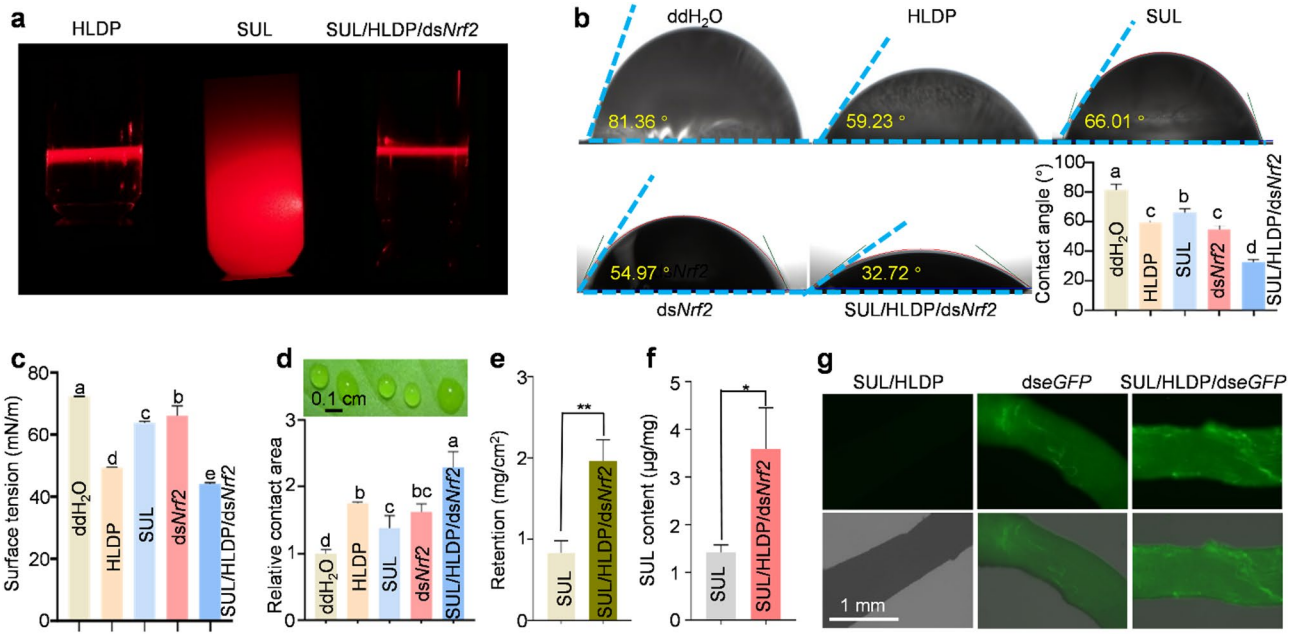

Fig. 5 Leaf adhesion, retention and plant uptake assay SUL/HLDP/ds*Nrf2* complex. **(a)** Tyndall effects of HLDP (based on the PCL toward SUL), SUL (0.1 mg/mL) and SUL/HLDP/ds*Nrf2* complex (SUL concentration: 0.1 mg/mL). **(b)** Contact angles of various formulations (SUL concentration: 0.1 mg/mL) on the cowpea leaves. Each treatment included three independent samples. Different letters above the bars indicate significant differences at $P < 0.05$ as determined by Duncan's multiple range test. **(c)** Surface tensions of various formulations (SUL concentration: 0.1 mg/mL). Each sample was measured three times consecutively. **(d)** Contact areas of various formulations (SUL concentration: 0.1 mg/mL) on the cowpea leaves. Each treatment included three independent samples. **(e)** Retention of SUL/HLDP/ds*Nrf2* complex (SUL concentration: 100 mg/L) on the cowpea leaves. Each treatment included three independent samples. The "*" and "**" indicate significant differences according to the independent *t*-test, respectively ($P < 0.05$ and $P < 0.01$). **(f)** Plant uptake of SUL/HLDP/ds*Nrf2* complex (SUL concentration: 0.2 mg/mL). Each treatment included three independent samples. **(g)** Root uptake of fluorescent ds*eGFP* delivered by HLDP (ds*eGFP*: 1 μg)

leaves, and the complexation with HLDP could promote the plant uptake of both SUL and dsRNA.

Excellent delivery of SUL/HLDP/dsNrf2 complex in vivo and in vitro

The fluorescent SUL/HLDP/ds*eGFP* complex was used to evaluate its delivery efficiency in BFT adult (in vivo) and *Drosophila* S2 cells (in vitro). The results showed that the relative fluorescence intensity of adults treated with SUL/HLDP/ds*eGFP* complex was 2.58, which was significantly higher than those with SUL/HLDP complex (1.00) and ds*eGFP* (1.07) (Fig. 6a). Meanwhile, the fluorescence intensity of *Drosophila* S2 cells incubated with the SUL/HLDP/ds*eGFP* complex for 6 h was 163.80 a.u., which was significantly higher than those with ds*eGFP* (118.31 a.u.) and SUL/HLDP complex (0 a.u.) (Fig. 6b). Furthermore, the fluorescence intensities of cells incubated with SUL/HLDP/ds*eGFP* complex, ds*eGFP* and SUL/HLDP complex for 12 h were 252.61, 215.87 and 0 a.u., respectively, indicating that the SUL/HLDP/ds*eGFP* complex could be effectively transported across the cell membrane into cytoplasm. The current results demonstrated that the SUL/HLDP/ds*Nrf2* complex exhibited excellent delivery capabilities both in vivo and in vitro, with their advantages summarized in Fig. 6c.

High insecticidal activity of SUL/HLDP/ds*Nrf2* complex via suppressing the detoxification

The LC_{50} value based on the toxicity regression equation of SUL against BFT adults was used to prepare various formulations, including SUL/HLDP complex, ds*Nrf2*/HLDP complex and SUL/HLDP/ds*Nrf2* complex, etc. (Table S3). Their insecticidal activities were examined through immersion method and oral feeding, respectively (Fig. 7a, f). The results showed that the ds*Nrf2*/HLDP complex had a slight lethal effect on BFT adults,

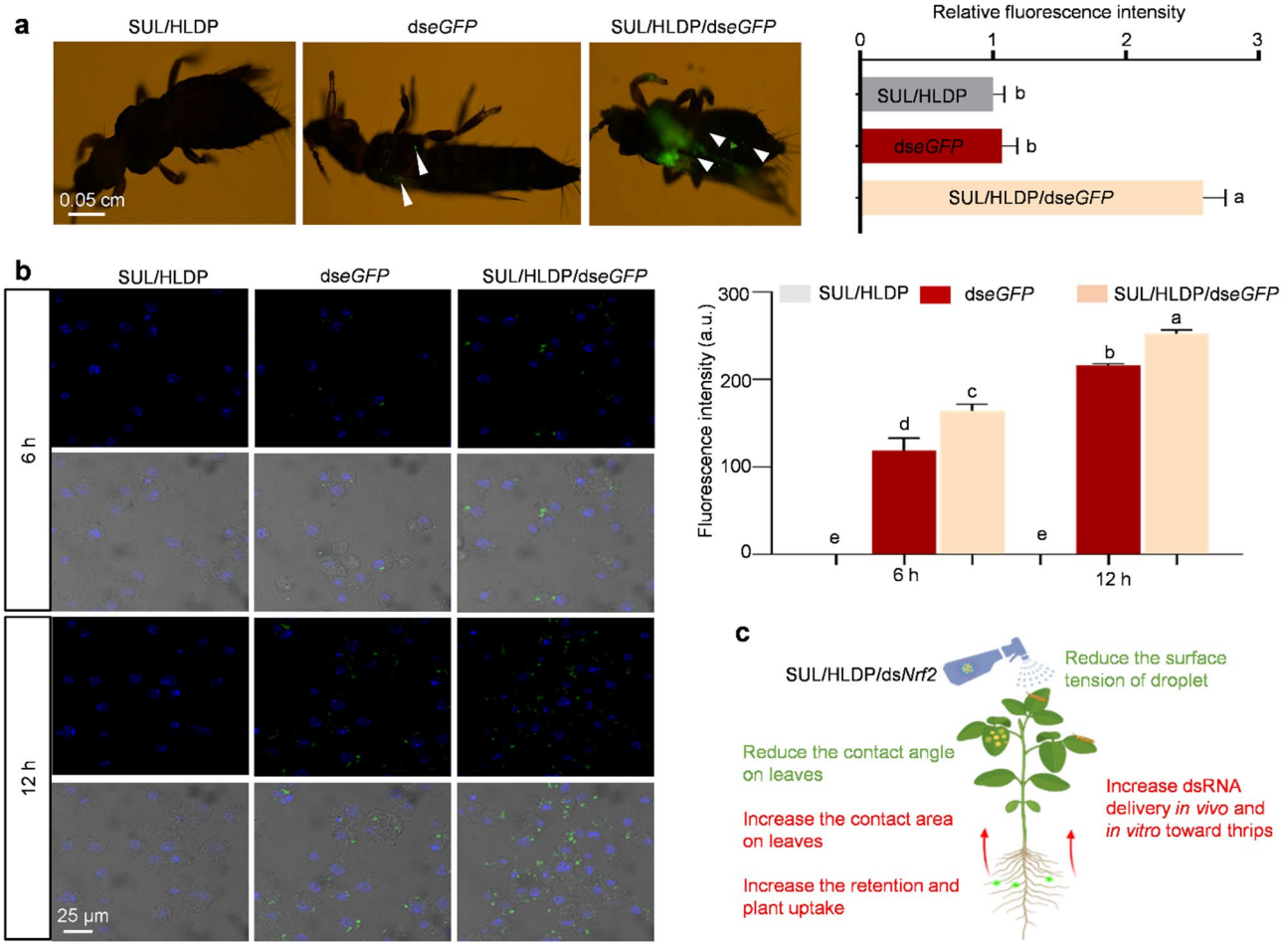

Fig. 6 Delivery efficiency assay of SUL/HLDP/ds*Nrf2* complex in vivo and in vitro. **(a)** Fluorescence intensities of BFT adults treated with various formulations (ds*eGFP*: 1 μg) through topical application. The fluorescence intensity was quantified using the ImageJ 1.8. Green: fluorescent ds*eGFP*. Each treatment included three biological replicates. **(b)** Fluorescence intensities of *Drosophila* S2 cells incubated with various formulations (ds*eGFP*: 1 μg). Blue: DAPI; Green: fluorescent ds*eGFP*. Each treatment included three biological replicates. Different letters above the bars indicate significant differences at $P < 0.05$ as determined by Duncan's multiple range test. **(c)** Summary diagram for better adhesion and delivery performance of SUL/HLDP/ds*Nrf2* complex

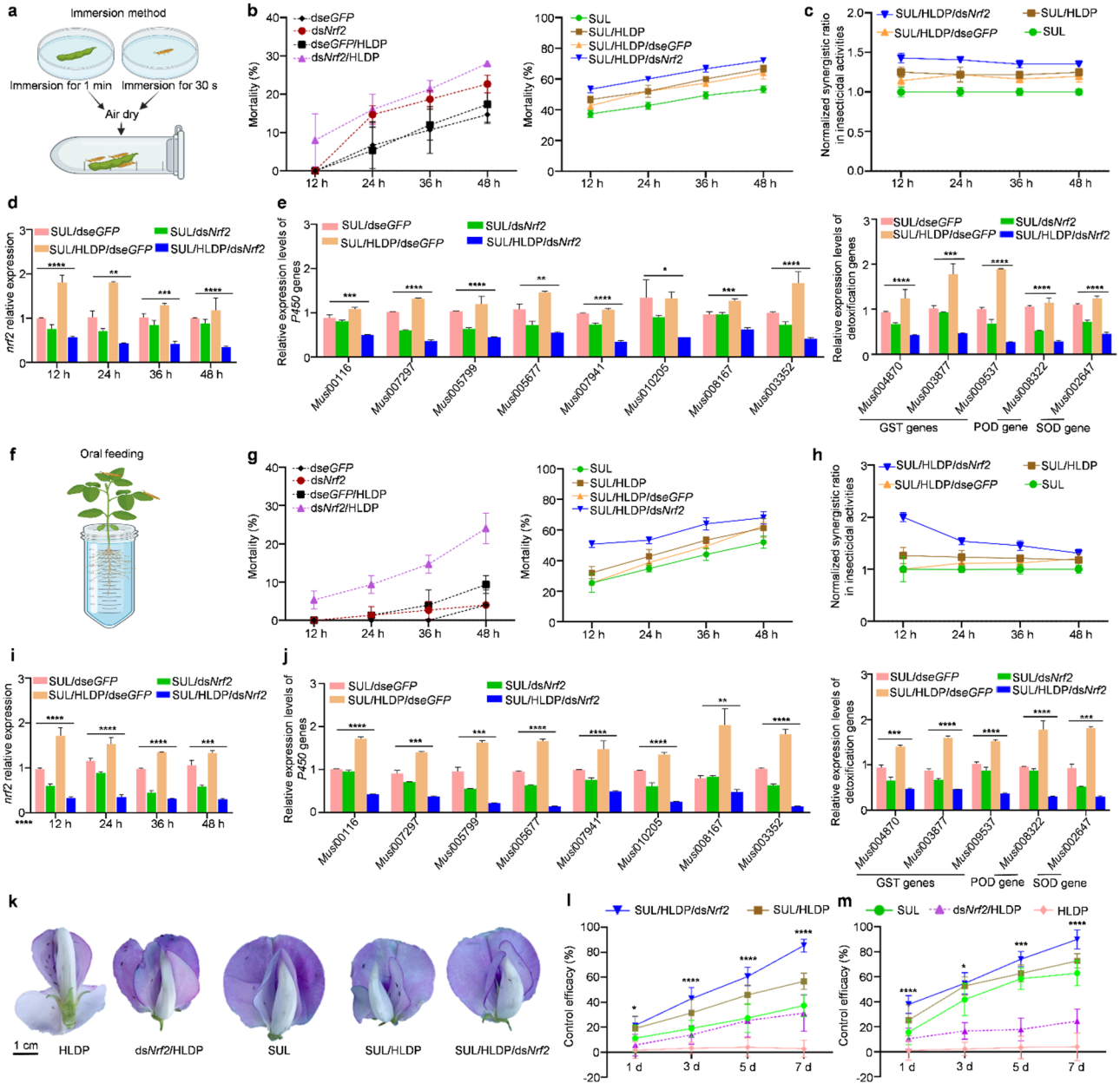

Fig. 7 Bioactivity and control efficacy of SUL/HLDP/ds*Nrf2* complex toward BFTs in the laboratory and field. **(a**, **f)** Diagram of immersion method (a) and oral feeding (f) for BFTs. **(b**, **g)** Mortalities of BFTs at 12, 24, 36 and 48 h after the immersion method (b) and oral feeding (g). The solutions included ds*eGFP* (0.219 mg/mL), ds*Nrf2* (0.219 mg/mL), ds*eGFP*/HLDP complex (0.219:0.876 mg/mL), ds*Nrf2*/HLDP complex (0.219:0.876 mg/mL), SUL (0.177 mg/mL), SUL/HLDP complex (0.177:0.876 mg/mL), SUL/HLDP/ds*eGFP* complex (0.177:0.876:0.219 mg/mL) and SUL/HLDP/ds*Nrf2* complex (0.177:0.876:0.219 mg/mL). The experiment was conducted in three replicates, with 30 adults per replicate. **(c**, **h)** Normalized synergistic ratios of SUL/HLDP/ds*Nrf2* complex toward BFTs through immersion method (c) and oral feeding (h). Three replicates were performed with a total of 30 adults in each replicate. **(d**, **i)** Expression levels of *nrf2* in the BFTs treated with SUL/ds*eGFP* complex (0.177:0.219 mg/mL), SUL/ds*Nrf2* complex (0.177:0.219 mg/mL), SUL/HLDP/ds*eGFP* complex (0.177:0.876:0.219 mg/mL) and SUL/HLDP/ds*Nrf2* complex (0.177:0.876:0.219 mg/mL), at 12, 24, 36 and 48 h after the immersion method (d) and oral feeding (i). Each treatment included three independent samples. **(e**, **j)** Expression levels of detoxification genes (*P450*, *GST*, *POD* and *SOD*) in the BFTs at 48 h via the immersion method (e) and oral feeding (j) of above solutions. Each treatment included three independent samples. **(k)** Control efficacy of SUL/HLDP/ds*Nrf2* complex (Actual content of SUL: 0.177 mg/mL) in field at 7 d after spraying. **(l**, **m)** Control efficacy of SUL/HLDP/ds*Nrf2* complex in the cowpea field of the Sanya Institute of Breeding and Multiplication, Hainan University (Actual content of SUL: 0.124 mg/mL) (l) and Sanya Institute of China Agricultural University (Actual content of SUL: 0.177 mg/mL) (m), respectively. The population density of BFT adults on cowpea flowers was about 30 per flower. Ten plants were selected from each plot as ten replicates, and the number of BFTs on the flowers was recorded at 0, 1, 3, 5 and 7 d after the treatment. The independent *t*-test was performed for the control efficacy of SUL/HLDP/ds*Nrf2* complex and SUL alone, and the "*", "**", "***" and "****" indicate significant differences ($P < 0.05$, $P < 0.01$, $P < 0.001$ and $P < 0.0001$)

with mortalities of 28% and 24% via immersion method and oral feeding, respectively (Fig. 7b, g). The contact and stomach toxicities of SUL/HLDP/ds*Nrf2* complex were the strongest among tested formulations at 48 h after the treatment, and the mortalities reached 72% and 68%, respectively, significantly higher than 53% and 52% with SUL alone. Moreover, the normalized synergistic ratios of SUL/HLDP/ds*Nrf2* complex were 1.35–1.43 and 1.31-2.00 compared to the SUL alone, respectively (Fig. 7c, h). Based on the toxicity regression equation (Table S3), the required doses of multicomponent RNA nano-biopesticide to achieve similar insecticidal activity were calculated, and its application doses were 50.14% and 58.42% of SUL via immersion method and oral feeding, respectively, suggesting that the application of HLDP could remarkably improve the bioactivity of SUL and reduce its application.

The expression of *nrf2* and detoxification genes (*P450*, *GST*, *POD* and *SOD*) was also examined in the BFTs treated with various formulations. For immersion method, the expression of *nrf2* in the BFTs treated with the SUL/HLDP/ds*Nrf2* complex decreased by 43.07%, 58.77%, 59.27% and 65.57% at 12, 24, 36 and 48 h, respectively compared to those with SUL/ds*eGFP* complex (Fig. 7d). Similarly, the oral feeding of SUL/HLDP/ds*Nrf2* complex also suppressed the expression of *nrf2* with reductions of 64.40%, 80.20%, 66.07% and 75.73%, respectively (Fig. 7i). Additionally, the RNAi efficiencies in the BFTs treated with SUL/HLDP/ds*Nrf2* complex were increased by 1.78, 1.85, 3.52 and 5.54 times than those treated with the mixture of SUL and ds*Nrf2* at 12, 24, 36 and 48 h after the immersion, and those were 1.72, 2.96, 1.24 and 1.61 times via oral feeding (Fig. 7d, i). As expected, the application of SUL/HLDP/ds*Nrf2* complex could also inhibit the expression of tested detoxification genes in BFTs (Fig. 7e, j).

Excellent control efficacy of SUL/HLDP/ds*Nrf2* complex in the field

The control efficacy of SUL/HLDP/ds*Nrf2* complex was evaluated in the field with the BFT population density of approximately 30 individuals per flower. As shown in Fig. 7k, BFT adults primarily hid in cowpea flowers, making their control extremely difficult. Cowpea flowers bloomed from 7 to 9 a.m, so it was crucial to seize the opportunity to control BFTs. The SUL/HLDP/ds*Nrf2* complex had the best control effect on the BFTs at 7 d after spraying (Fig. 7k). The SUL/HLDP/ds*Nrf2* complex exhibited slow-acting characteristics, with its control efficacy gradually increasing to 85.36% (Fig. 7l) and 89.89% (Fig. 7m) at 7 d after spraying, which was significantly higher than those of SUL/HLDP complex (56.74% in Figs. 7l and 72.66% in Fig. 7m), SUL alone (37.31% in Figs. 7l and 62.88% in Fig. 7m), and ds*Nrf2*/HLDP complex (31.36% in Figs. 7l and 24.56% in Fig. 7m), respectively. Additionally, the control efficacy of SUL/HLDP/ds*Nrf2* complex was significantly higher than that of SUL alone at 1, 3, 5 and 7 d after spraying (Fig. 7l, m). As expected, the application of HLDP could not control BFTs with the final control efficacy of merely 2.87% (Fig. 7l) and 3.98% (Fig. 7m). According to the current data, the application of SUL/HLDP/ds*Nrf2* complex could inhibit the detoxification and metabolism of BFTs and improve their sensitivity to SUL for better control effects.

Discussion

As a key transcription factor regulating oxidative stress, Nrf2 binds to the antioxidant response elements to induce the expression of cytoprotective genes under stress conditions [14–16, 18, 44]. In the current study, RNA-seq analysis showed that the DEGs were mainly enriched in detoxification-related pathways after the down-regulation of *nrf2*. The RNAi of *nrf2* suppressed the expression of detoxification genes, such as the genes in CYP3, 4 and 6 subfamilies of the P450 family, GSTs, PODs and SODs, and the activities of corresponding detoxifying enzymes were also reduced. This is consistent with the *Drosophila* results that *nrf2* gene regulates the expression of detoxification genes, including 36 cytochrome P450 genes, 17 GST genes, 6 UGT genes and 55 predictive transmembrane transporter genes [45]. These detoxification genes play important roles in the transformation and metabolism of toxic substances, detoxification of lipophilic compounds, and maintenance of oxidative balance within the body [13, 46–48]. Previous researches have indicated that the down-regulation of above detoxification genes increases the insect sensitivity to pesticides [49–51]. For instance, the RNAi of some genes in CYP4 subfamily can lead to the reduction in oxidase activity and insecticide resistance in *Diaphorina citri* and *Blattella germanica* [50, 52]. Down-regulation of key resistance-related genes (*GSTe3*, *CYP9A121* and *CYP9A122*) can significantly decrease the tolerance of *Cydia pomonella* to lambda-cyhalothrin [53]. Therefore, our results demonstrated that the Nrf2 could be applied as a promising target for increasing the susceptibility of BFTs to insecticides.

The HLDP nanocarrier was designed and developed to prepare a nanoscale SUL/HLDP/ds*Nrf2* complex, and its self-assembly mechanism was analyzed using a widely-adopted method ITC [40, 54]. The HLDP could spontaneously assemble with SUL via hydrogen bonds and Van der Waals forces into SUL/HLDP complex, which further combined with ds*Nrf2* via electrostatic interaction, hydrogen bonds, etc. Interestingly, our UPLC data demonstrated that the HLDP could load SUL and ds*Nrf2* simultaneously, and the optimal mass ratio of SUL:

HLDP: ds*Nrf2* was calculated to be 14:69:17. The cationic HLDP possesses both hydrophobic and hydrophilic functional groups to allow it to assemble with various types of substances. Similarly, the SPc nanocarrier can bind with exogenous substances via various types of interaction forces, such as electrostatic interaction, hydrogen bond, hydrophobic interaction, Van der Waals force, etc [27, 55–57]. For instance, the cellobiose or matrine can be loaded into the hydrophobic core of SPc, which can further assemble with dsRNA via electrostatic interaction, hydrogen bond, etc. to form pesticide/SPc/dsRNA complex [33, 58]. A recent publication has reported that the self-assembly of HLDP-salicylic acid (SA) protectant is primarily driven by electrostatic interactions, and the complexation with the HLDP decreases the particle size of SA down to 67 nm [32]. The current study revealed that the SUL/HLDP/ds*Nrf2* complex consisted of nanoscale spherical particles, and its particle size was slightly larger than that of SUL/HLDP complex, which might be due to the electrostatic adhesion of ds*Nrf2* on the surface of SUL/HLDP complex. The pesticide nanometerization is very common, and the assembly with SPc can decrease the particle sizes of osthol, thiamethoxam and chitosan from 289 to 18 nm, from 576 to 116 nm and from 145 to 17 nm, respectively [55–57].

The fundamental properties of pesticide droplets, such as contact angle, surface tension and contact area, are key factors influencing the plant uptake and insecticidal activity [59]. Previous studies have shown that the smaller particle size of nano-pesticides is conductive to expanding the contact area with pests, improving pesticide deposition, and increasing plant bioavailability [60, 61]. Our results revealed that the SUL/HLDP/ds*Nrf2* complex displayed the best leaf adhesion performance among tested formulations, with the smaller contact angle, reduced surface tension, amplified contact area, improved retention, and enhanced plant uptake. A recent publication has reported that the contact angle of SA can decrease by 6.8° with the aid of HLDP, and its retention increases by 4.1 mg/cm², indicating that the complexation with HLDP can reduce the surface tension of drug droplets, promote their diffusion and adhesion, and thus increase their retention [32]. Similarly, previous studies have demonstrated that the contact angle of SPc-loaded pesticides significantly decreases, and their plant uptake increases by 1.45–1.53 and 1.9–2.4 times, respectively [29, 62].

The nanoscale SUL/HLDP/ds*Nrf2* complex exhibited excellent delivery efficiencies both in vitro and in vivo. Nanomaterials, such as polymers and nanomicelle, can protect nucleic molecules from enzymatic degradation and promote cellular uptake [63, 64]. Previous research has also confirmed that the SPc can up-regulate some critical genes to activate the endocytosis and exocytosis pathways for enhanced cellular uptake [27]. For instance, the SPc-loaded dsRNA can penetrate the physical obstacles of eggshell and larval body wall of fall armyworms for efficient delivery [65]. The matrine/SPc/dsRNA complex can be efficiently delivered into *Drosophila* S2 cells compared with naked dsRNA [33]. So far, the SPc-mediated dsRNA delivery system has been successfully applied in more than 30 insect species, and the current study also provided an efficient HLDP-based nano-platform for delivering both dsRNA and pesticides.

The insecticidal activity of SUL was significantly improved with the aid of HLDP, and the application of SUL/HLDP/ds*Nrf2* complex exhibited the strongest lethal effect on the BFTs. Similarly, previous studies have demonstrated that the application of nanocarrier co-loaded with dsRNA and insecticide exhibit excellent insecticidal activity and control efficacy against green peach aphids and fall armyworms [33, 66]. A recent publication has also reported that the HLDP-SA nano-protectant displays the best control effects on cotton Verticillium wilt [32]. In the current study, we also demonstrated that the application of SUL/HLDP/ds*Nrf2* complex could suppress the expression of *nrf2* and detoxification genes (*P450*, *GST*, *POD* and *SOD*) in BFTs, thus it could be applied to increase the susceptibility of BFTs to insecticides. Consistent with previous studies, the *nrf2* RNAi can inhibit the expression of downstream detoxification genes, thereby increasing the sensitivity of insects to pesticides [49–51]. For instance, Nrf2 can bind to the promoter of GST to up-regulate its expression, thereby enabling *Spodoptera litura* to respond to exogenously-induced reactive oxygen species and protect cells from exogenous toxicity [49]. The *nrf2* RNAi can significantly down-regulate the expression of *CYP6FD1* and *CYP6FE1* in *Locusta migratoria*, which is able to increase its sensitivity to deltamethrin and imidacloprid [67]. Similarly, knockdown of *nrf2* significantly inhibits the expression of *CYP321A1* and reduces the tolerance of *Helicoverpa armigera* larvae to flavone [68]. Additionally, we have not yet obtained the resistant populations of BFTs, which limits further verification of SUL/HLDP/ds*Nrf2* complex effects on metabolic resistance in SUL-resistant BFTs. Overall, this study elucidated the regulatory role of *nrf2* in the detoxification and metabolism of BFTs and developed a self-assembled multicomponent RNA nanobiopesticide to increase the susceptibility of BFTs to insecticides.

Conclusions

To enhance the susceptibility of destructive BFTs to insecticides, we firstly demonstrated the crucial regulatory role of *nrf2* in the expression of antioxidant and detoxifying enzyme genes, and the down-regulation of *nrf2* could remarkably suppress the expression of most

detoxification genes and the activity of various detoxifying enzymes. Then, we designed and constructed a novel HLDP-based co-delivery nano-platform, which was applied to develop a self-assembled multicomponent RNA nano-biopesticide (SUL/HLDP/ds*Nrf2* complex) toward BFTs. The multicomponent RNA nano-biopesticide achieved the self-assembly via hydrogen bonds, Van der Waals forces and electrostatic interactions to form nanoscale particles. The multicomponent RNA nano-biopesticide displayed better adhesion performance on plant leaves with smaller contact angle, reduced surface tension, amplified contact area, increased retention, and stronger plant uptake. Meanwhile, its delivery efficiency was remarkably improved in vitro and in vivo. Notably, the multicomponent RNA nano-biopesticide achieved excellent insecticidal activity and control efficacy toward BFTs via suppressing *nrf2* expression. Overall, this study developed a self-assembled multicomponent RNA nano-biopesticide to increase insecticidal activity, which provided a revolutionary strategy for designing and developing novel pesticides/drugs for resistance management.

Supplementary Information

The online version contains supplementary material available at https://doi.org/10.1186/s12951-025-03460-5.

Supplementary Material 1

Acknowledgements

This work was supported by the Project of Sanya Yazhou Bay Science and Technology City (SCKI-JYRC-2022-26), National Natural Science Foundation of China (32372631), Postdoctoral Fellowship Program (Grad C) of China Postdoctoral Science Foundation (GZC20233041), Hainan Provincial Natural Science Foundation of China (325QN395) and Pinduoduo-China Agricultural University Research Fund (PC2023B02018).

Author contributions

JZ: Design, Experiment, Methodology, Writing—original draft. ZW, JY and YW: Methodology. ML and ZM: Visualization. MY, MD and JS: Resources, Conceptualization and Supervision. SY: Design, Conceptualization, Resources, Supervision, Review and Editing.

Data availability

Data is provided within the manuscript or supplementary information files.

Declarations

Ethics approval and consent to participate

Not applicable.

Consent for publication

All authors agreed to publish this manuscript.

Competing interests

The authors declare no competing interests.

Received: 17 March 2025 / Accepted: 11 May 2025
Published online: 20 May 2025

References

1. Huan Z, Xu Z, Luo J, Xie D. Monitoring and exposure assessment of pesticide residues in Cowpea (*Vigna unguiculata* L. Walp) from five provinces of Southern China. Regul Toxicol Pharmacol. 2016;81:260–7.
2. Tang D, Guo LH, Ali A, Desneux N, Zang LS. Synergism of adjuvants mixed with Spinetoram for the management of bean flower thrips, *Megalurothrips usitatus* (Thysanoptera: Thripidae) in Cowpeas. J Econ Entomol. 2022;115:2013–9.
3. Watson GB, Siebert MW, Wang NX, Loso MR, Sparks TC. Sulfoxaflor-a sulfoximine insecticide: review and analysis of mode of action, resistance and crossresistance. Pestic Biochem Physiol. 2021;178:104924.
4. Sparks TC, Watson GB, Loso MR, Geng CX, Babcock JM, Thomas JD. Sulfoxaflor and the sulfoximine insecticides: chemistry, mode of action and basis for efficacy on resistant insects. Pestic Biochem Physiol. 2013;107:1–7.
5. Huan ZB, Yu SX, Wang MY. Field efficacy of 4 insecticides to control *Megalurothrips usitatus* Bagnall and *Liriomyza sativae* Blanchard in Hainan Cowpea. Agrochemicals. 2023;62:530–3.
6. Yu FQ, Huang YS, Su Z, Wu EM, Wang Z, Yu CR. A novel insecticides sulfoxaflor. Agrochemicals. 2013;52:753–5.
7. Ma L, Liu Q, Wei S, Liu SL, Tian L, Song F, Duan Y, Cai W, Li H. Chromosome-level genome assembly of bean flower thrips *Megalurothrips usitatus* (Thysanoptera: Thripidae). Sci Data. 2023;10:252.
8. Mouden S, Sarmiento KF, Klinkhamer PGL, Leiss KA. Integrated pest management in Western flower Thrips: past, present and future. Pest Manag Sci. 2017;73:813–22.
9. Brattsten LB, Holyoke CW, Leeper JR, Raffa KF. Insecticide resistance: challenge to pest management and basic research. Science. 1986;231:1255–60.
10. Pang R, Wang J, Li H, Zhong Z, Li Z, Qiu B, Zhou C, Alia S, Wu J. Identification of the cypome associated with Acetamiprid resistance based on the chromosome-level genome of *Megalurothrips usitatus* (Bagnall) (Thysanoptera: Thripidae). Pest Manag Sci. 2025;81:3273–83.
11. Sparks TC, DeBoer GJ, Wang NX, Hasler JM, Loso MR, Watson GB. Differential metabolism of sulfoximine and neonicotinoid insecticides by *Drosophila melanogaster* monooxygenase CYP6G1. Pestic Biochem Physiol. 2012;103:159–65.
12. Wilding C. Regulating resistance: CncC: Maf, antioxidant response elements and the overexpression of detoxification genes in insecticide resistance. Curr Opin Insect Sci. 2018;27:89–96.
13. Nauen R, Bass C, Feyereisen R, Vontas J. The role of cytochrome P450s in insect toxicology and resistance. Annu Rev Entomol. 2022;67:105–24.
14. Hirotsu Y, Katsuoka F, Funayama R, Nagashima T, Nishida Y, Nakayama K, Engel JD, Yamamoto M. Nrf2-MafG heterodimers contribute globally to antioxidant and metabolic networks. Nucleic Acids Res. 2012;40:10228–39.
15. Ma Q. Role of Nrf2 in oxidative stress and toxicity. Annu Rev Pharmacol Toxicol. 2013;53:401–26.
16. Loboda A, Damulewicz M, Pyza E, Jozkowicz A, Dulak J. Role of Nrf2/HO-1 system in development, oxidative stress response and diseases: an evolutionarily conserved mechanism. Cell Mol Life Sci. 2016;73:3221–47.
17. Tonelli C, Chio IIC, Tuveson DA. Transcriptional regulation by Nrf2. Antioxid Redox Signal. 2018;29:1727–45.
18. Ko E, Kim D, Min DW, Kwon SH, Lee JY. Nrf2 regulates cell motility through RhoA-ROCK1 signalling in non-small-cell lung cancer cells. Sci Rep. 2021;11:1247.
19. Luo X, Nanda S, Zhang Y, Zhou X, Yang C, Pan H. Risk assessment of RNAi-based biopesticides. New Crops. 2024;1:100019.
20. Fletcher SJ, Reeves PT, Hoang BT, Mitter N. A perspective on RNAi-based biopesticides. Front Plant Sci. 2020;11:51.
21. Shaffer L. RNA-based pesticides aim to get around resistance problems. PNAS. 2020;117:32823–6.
22. Liu S, Jaouannet M, Dempsey DMA, Imani J, Coustau C, Kogel KH. RNA-based technologies for insect control in plant production. Biotechnol Adv. 2020;39:107463.
23. Usman M, Farooq M, Wakeel A, Nawaz A, Cheema SA, Rehman H, Ashraf I, Sanaullah M. Nanotechnology in agriculture: current status, challenges and future opportunities. Sci Total Environ. 2020;721:137778.
24. Rodrigues SM, Demokritou P, Dokoozlian N, Hendren CO, Karn B, Mauter MS, Sadik OA, Safarpour M, Unrine JM, Viers J, Welle P, White JC, Wiesner MR, Lowry GV. Nanotechnology for sustainable food production: promising opportunities and scientific challenges. Environ Sci Nano. 2017;4:767–81.
25. Gilbertson LM, Pourzahedi L, Laughton S, Gao X, Zimmerman J, Theis T, Westerhoff P, Lowry GV. Guiding the design space for nanotechnology to advance sustainable crop production. Nat Nanotechnol. 2020;15:801–10.

26. Majumder J, Minko T. Multifunctional and stimuli-responsive nanocarriers for targeted therapeutic delivery. Expert Opin Drug Del. 2021;18:205–27.
27. Ma Z, Zheng Y, Chao Z, Chen H, Zhang Y, Yin M, Shen J, Yan S. Visualization of the process of a nanocarrier-mediated gene delivery: stabilization, endocytosis and endosomal escape of genes for intracellular spreading. J Nanobiotechnol. 2022;20:124.
28. Zhang Y, Fu L, Li S, Yan J, Sun M, Giraldo J, Matyjaszewski K, Tilton RD, Lowry GV. Star polymer size, charge content, and hydrophobicity affect their leaf uptake and translocation in plants. Environ Sci Technol. 2021;55:10758–68.
29. Jiang Q, Xie Y, Peng M, Wang Z, Li T, Yin M, Shen J, Yan S. A nanocarrier pesticide delivery system with promising benefits in the case of Dinotefuran: strikingly enhanced bioactivity and reduced pesticide residue. Environ Sci Nano. 2022;9:988–99.
30. Xiao S, Shoaib A, Xu J, Lin D. Mesoporous silica size, charge, and hydrophobicity affect the loading and releasing performance of lambda-cyhalothrin. Sci Total Environ. 2022;831:154914.
31. Peng PH, Jian J, Long H, Jiang Q, Huang W, Kong L, Yin M, Su XF, Peng DL, Yan S. Self-assembled nanonematicide induces adverse effects on oxidative stress, succinate dehydrogenase activity, and ATP generation. ACS Appl Mater Interfaces. 2023;15:31173–84.
32. Yin JM, Zhao JJ, Wang Z, Xue F, Wang Q, Guo HM, Cheng HM, Li J, Shen J, Yin MZ, Su XF, Yan S. Preparation of Salicylic acid nano-protectant with dual synergistic mechanism: high direct fungicidal activity and plant defence toward cotton verticillium wilt. Chem Eng J. 2024;496:154036.
33. Li MS, Ma Z, Peng M, Li L, Yin M, Yan S, Shen J. A gene and drug co-delivery application helps to solve the short life disadvantage of RNA drug. Nano Today. 2022;43:101452.
34. Zhao J, Yan S, Li M, Sun L, Dong M, Yin M, Shen J, Zhao ZW. NPFR regulates the synthesis and metabolism of lipids and glycogen via AMPK: novel targets for efficient corn borer management. Int J Biol Macromol. 2023;247:125816.
35. Livak KJ, Schmittgen TD. Analysis of relative gene expression data using real-time quantitative PCR and the $2^{-\Delta\Delta CT}$ method. Methods. 2001;25:402–8.
36. Bray NL, Pimentel H, Melsted P, Pachter L. Near-optimal probabilistic RNA-seq quantification. Nat Biotechnol. 2016;34:525–7.
37. Kanehisa M, Susumu G. KEGG: Kyoto encyclopedia of genes and genomes. Nucleic Acids Res. 2000;28:27–30.
38. Feingold EA, Good PJ, Guyer MS, Kamholz S, Liefer L, Wetterstrand K, Collins FS. The ENCODE (ENCyclopedia of DNA elements) project. Science. 2004;306:636–40.
39. Ma ZZ, Zhou H, Wei YL, Yan S, Shen J. A novel plasmid-Escherichia coli system produces large batch DsRNAs for insect gene Silencing. Pest Manag Sci. 2020;76:2505–12.
40. Doyle ML. Characterization of binding interactions by isothermal Titration calorimetry. Curr Opin Biotechnol. 1997;8:31–5.
41. Cheng Y, Ou X, Ma J, Sun L, Ma Z. A new amphiphilic Brønsted acid as catalyst for the friedel-crafts reactions of Indoles in water. Eur J Org Chem. 2019;2019:66–72.
42. Zheng L, Cao C, Cao LD, Chen Z, Huang QL, Song BA. Bounce behavior and regulation of pesticide solution droplets on rice leaf surfaces. J Agric Food Chem. 2018;66:11560–8.
43. Ross PD, Subramanian S. Thermodynamics of protein association reactions: forces contributing to stability. Biochemistry. 1981;20:3096–102.
44. Krajka-Kuźniak V, Paluszczak J, Baer-Dubowska W. The Nrf2-ARE signaling pathway: an update on its regulation and possible role in cancer prevention and treatment. Pharmacol Rep. 2017;69:393–402.
45. Misra JR, Horner MA, Lam G, Thumme CS. Transcriptional regulation of xenobiotic detoxification in *Drosophila*. Genes Dev. 2011;25:1796–806.
46. Pavlidi N, Vontas J, Van Leeuwen T. The role of glutathione S-transferases (GSTs) in insecticide resistance in crop pests and disease vectors. Curr Opin Insect Sci. 2018;27:97–102.
47. Kobayashi Y, Nojima Y, Sakamoto T, Iwabuchi K, Nakazato T, Bono H, Toyoda A, Fujiyama A, Kanost MR, Tabunoki H. Comparative analysis of seven types of superoxide dismutases for their ability to respond to oxidative stress in *Bombyx mori*. Sci Rep. 2019;9:2170.
48. Kaur S, Samota MK, Choudhary M, Choudhary M, Pandey AK, Sharma A, Thakur J. How do plants defend themselves against pathogens-Biochemical mechanisms and genetic interventions. Physiol Mol Biol Plants. 2022;28:485–504.
49. Chen S, Lu M, Zhang N, Zou X, Mo M, Zheng S. Nuclear factor erythroid-derived 2-related factor 2 activates glutathione S-transferase expression in the midgut of *Spodoptera litura* (Lepidoptera: Noctuidae) in response to phytochemicals and insecticides. Insect Mol Biol. 2018;27:522–32.
50. Chen N, Pei XJ, Li S, Fan Y, Liu T. Involvement of integument-rich *CYP4G19* in hydrocarbon biosynthesis and cuticular penetration resistance in *Blattella germanica* (L). Pest Manag Sci. 2020;76:215–26.
51. He F, Ru X, Wen T. NRF2, a transcription factor for stress response and beyond. Int J Mol Sci. 2020;21:4777.
52. Killiny N, Hajeri S, Tiwari S, Gowda S, Stelinski L. Double-stranded RNA uptake through topical application, mediates Silencing of five *CYP4* genes and suppresses insecticide resistance in *Diaphorina citri*. PLoS ONE. 2014;9:e110536.
53. Hu C, Liu YX, Zhang SP, Wang YQ, Gao P, Li YT, Yang XQ. Transcription factor AhR regulates glutathione S-transferases conferring resistance to lambda-Cyhalothrin in *Cydia Pomonella*. J Agr Food Chem. 2023;71:5230–9.
54. Grolier JPE, del Río JM. Isothermal Titration calorimetry: A thermodynamic interpretation of measurements. J Chem Thermodyn. 2012;5:193–202.
55. Yan S, Hu Q, Jiang Q, Chen H, Wei J, Yin M, Du XG, Shen J. Simple osthole/nanocarrier pesticide efficiently controls both pests and diseases fulfilling the need of green production of strawberry. ACS Appl Mater Inter. 2021;13:36350–60.
56. Yan S, Cheng WY, Han ZH, Wang D, Yin MZ, Du XG, Shen J. Nanometerization of Thiamethoxam by a cationic star polymer nanocarrier efficiently enhances the contact and plant-uptake dependent stomach toxicity against green Peach aphids. Pest Manag Sci. 2021;77:1954–62.
57. Wang X, Zheng K, Cheng W, Li J, Liang X, Shen J, Dou DL, Yin MZ, Yan S. Field application of star polymer-delivered Chitosan to amplify plant defense against potato late blight. Cheml Eng J. 2021;417:129327.
58. Wang Y, Li M, Ying J, Shen J, Dou D, Yin M, Whisson SC, Birch PRJ, Yan S, Wang XD. High-efficiency green management of potato late blight by a self-assembled multicomponent nano-bioprotectant. Nat Commun. 2023;14:5622.
59. Bao Z, Wu Y, Song R, Gao Y, Zhang S, Zhao K, Wu TY, Zhang CH, Du FP. The simple strategy to improve pesticide bioavailability and minimize environmental risk by effective and ecofriendly surfactants. Sci Total Environ. 2022;851:158169.
60. Cao C, Liu M, Ma X, Chen Y, Huang Q. Enhancing droplets deposition on superhydrophobic plant leaves by bio-based surfactant: experimental characterization and molecular dynamics simulations. J Mol Liq. 2023;387:122696.
61. Tang J, Tong X, Chen Y, Wu Y, Zheng Z, Kayitmazer AB, Ahmad A, Ramzan N, Yang J, Huang QC, Xu YS. Deposition and water repelling of temperature-responsive nanopesticides on leaves. Nat Commun. 2023;14:6401.
62. Wang Y, Xie YH, Jiang QH, Chen HT, Ma RH, Wang ZJ, Yin MZ, Shen J, Yan S. Efficient polymer-mediated delivery system for thiocyclam: nanometerization remarkably improves the bioactivity toward green Peach aphids. Insect Sci. 2023;30:2–14.
63. Li C, Zhou J, Wu Y, Dong Y, Du L, Yang T, Wang YH, Guo S, Zhang MJ, Hussain A, Xiao HH, Weng YH, Huang Y, Wang XX, Liang ZC, Cao HQ, Zhao YX, Liang XJ, Dong AJ, Huang YY. Core role of hydrophobic core of polymeric nanomicelle in endosomal escape of SiRNA. Nano Lett. 2021;21:3680–9.
64. Yang T, Huang D, Li C, Zhao D, Li J, Zhang M, Chen YF, Wang Q, Liang ZC, Liang XJ, Li ZH, Huang YY. Rolling microneedle electrode array (RoMEA) empowered nucleic acid delivery and cancer immunotherapy. Nano Today. 2021;36:101017.
65. Chao Z, Ma Z, Zhang Y, Yan S, Shen J. Establishment of star polycation-based RNA interference system in all developmental stages of fall armyworm *Spodoptera frugiperda*. Entomol Gen. 2023;43:127–37.
66. Yan S, Li M, Jiang Q, Li M, Hu M, Shi X, Liang P, Yin MZ, Gao XW, Shen J, Zhang L. Self-assembled co-delivery nanoplatform for increasing the broad-spectrum susceptibility of fall armyworm toward insecticides. J Adv Res. 2025;67:93–104.
67. Liu J, Wu H, Zhang Y, Zhang J, Ma EB, Zhang X. Transcription factors, cap 'n'collar isoform C regulates the expression of *CYP450* genes involving in insecticides susceptibility in *Locusta migratoria*. Pestic Biochem Phys. 2023;196:105627.
68. Zhang C, Wang X, Tai S, Qi L, Yu X, Dai W. Transcription factor CncC potentially regulates cytochrome P450 *CYP321A1*-mediated flavone tolerance in *Helicoverpa armigera*. Pestic Biochem Phys. 2023;191:105360.

Publisher's note